

Tactile SoftHand-A: 3D-Printed, Tactile, Highly-underactuated, Anthropomorphic Robot Hand with an Antagonistic Tendon Mechanism

Journal Title
 XX(X):1–16
 ©The Author(s) 2024
 Reprints and permission:
 sagepub.co.uk/journalsPermissions.nav
 DOI: 10.1177/ToBeAssigned
 www.sagepub.com/

SAGE

Haoran Li¹, Christopher J. Ford¹, Chenghua Lu¹, Yijiong Lin¹, Matteo Bianchi², Manuel G. Catalano³, Efi Psomopoulou^{*1} and Nathan F. Lepora^{*1}

Abstract

For tendon-driven multi-fingered robotic hands, ensuring grasp adaptability while minimizing the number of actuators needed to provide human-like functionality is a challenging problem. Inspired by the Pisa/IIT SoftHand, this paper introduces a 3D-printed, highly-underactuated, five-finger robotic hand named the Tactile SoftHand-A, which features only two actuators. The dual-tendon design allows for the active control of specific (distal or proximal interphalangeal) joints to adjust the hand's grasp gesture. We have also developed a new design of fully 3D-printed tactile sensor that requires no hand assembly and is printed directly as part of the robotic finger. This sensor is integrated into the fingertips and combined with the antagonistic tendon mechanism to develop a human-hand-guided tactile feedback grasping system. The system can actively mirror human hand gestures, adaptively stabilize grasp gestures upon contact, and adjust grasp gestures to prevent object movement after detecting slippage. Finally, we designed four different experiments to evaluate the novel fingers coupled with the antagonistic mechanism for controlling the robotic hand's gestures, adaptive grasping ability, and human-hand-guided tactile feedback grasping capability. The experimental results demonstrate that the Tactile SoftHand-A can adaptively grasp objects of a wide range of shapes and automatically adjust its gripping gestures upon detecting contact and slippage. Overall, this study points the way towards a class of low-cost, accessible, 3D-printable, underactuated human-like robotic hands, and we openly release the designs to facilitate others to build upon this work. This work is Open-sourced at github.com/SoutheastWind/Tactile_SoftHand_A

Keywords

Multi-fingered robot hand, Underactuated robots, Mechanism design, Tactile sensing, Grasp synergies

Introduction

Anthropomorphic robotic hands can be used in various ways, such as for grasping/pick-and-place, remote teleoperation, autonomous in-hand manipulation and as prosthetics. However, developing economical and accessible anthropomorphic robotic hands that can approach the tactile sensibility and rich functionality of human hands has always been one of the most difficult and potentially rewarding challenges in robotics. The use of underactuated mechanisms is particularly appealing due to their simple structure, ease of maintenance, low cost, straightforward control, and adaptability to conform to the shape of objects (Piazza et al. (2019); Ozawa et al. (2014)). However, there are many such mechanisms for driving underactuated soft anthropomorphic hands, including pneumatic (Zhu et al. (2023), Lu et al. (2024)), tendon driven (Chen et al. (2018); Catalano et al. (2014); Li et al. (2022); Mizushima et al. (2018)) and linkage driven (Kim et al. (2020)).

Another important, but perhaps underappreciated, design aspect of anthropomorphic underactuated hands is the extension, or reset, of the finger joints, which plays a crucial role in the dexterity of the hand. Clearly, the human hand has different tendons to close and open the hand according to agonist and antagonist muscle groups. Fully

actuated robotic hands realize the bending and reset of the joints through the forward and reverse rotation of the motor at the joint (Butterfaß et al. (2001)). However, almost all tendon-underactuated robot hands use passive elastic elements (Makino et al. (2017); Martin and Grossard (2014)) such as rubber bands (Catalano et al. (2014); Li et al. (2022); Ma and Dollar (2017)), torsion springs (Mnyusiwalla et al. (2016); Li et al. (2017); Jiang et al. (2014); Mizushima et al. (2018); Stuart et al. (2017)) or soft continuous materials (Mohd Faudzi et al. (2018)) to reset the finger joints (Ozawa et al. (2014)).

The primary advantage of using passive elastic components lies in the significant reduction of integration and control complexity. However, this approach restricts control

¹School of Engineering Mathematics and Technology, and Bristol Robotics Laboratory, University of Bristol, Bristol, U.K.

² Department of Information Engineering and the Research Center "E.Piaggio", University of Pisa, Italy.

³ Soft Robotics for Human Cooperation and Rehabilitation, Istituto Italiano di Tecnologia (IIT), Italy.

Corresponding author:

Nathan F. Lepora, School of Engineering Mathematics and Technology, and Bristol Robotics Laboratory, University of Bristol, Bristol, U.K.
 Email: n.lepora@bristol.ac.uk

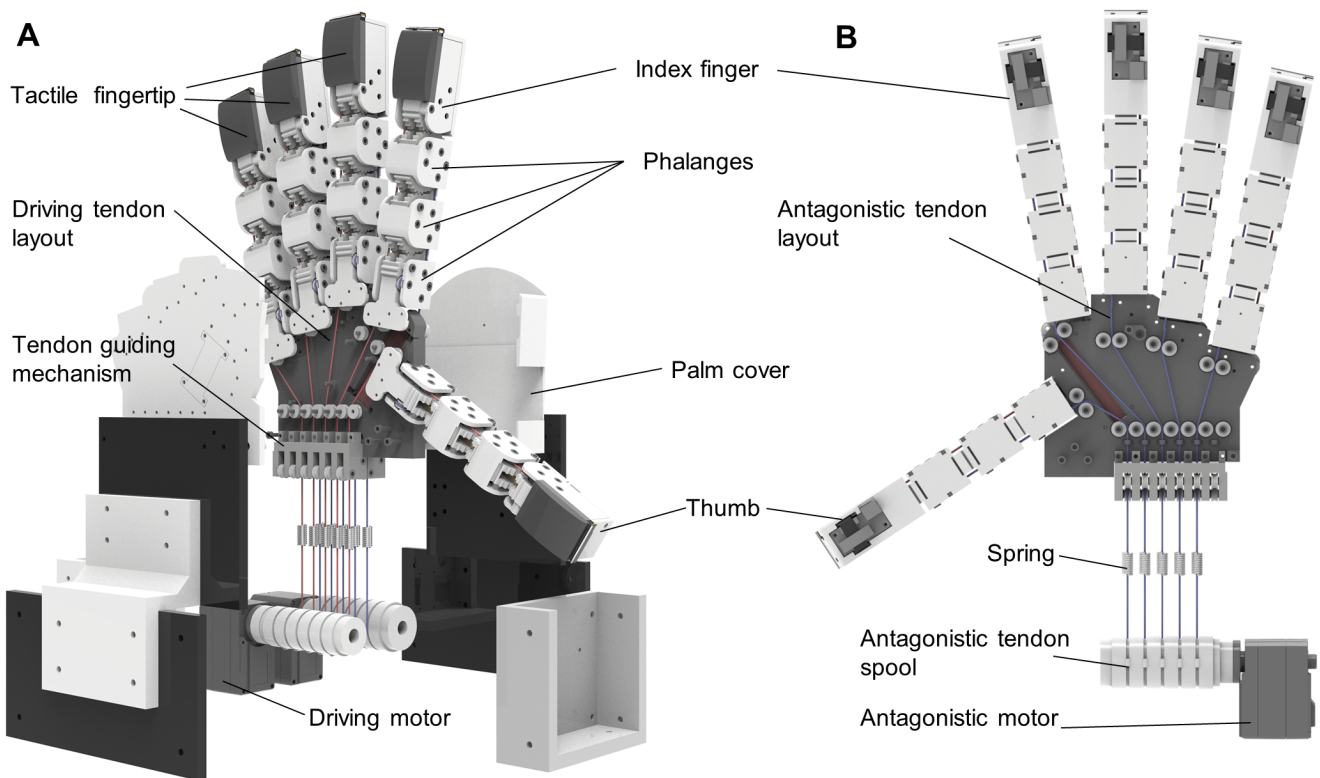


Figure 1. Exploded Front view (A) and back view (B) of the Tactile SoftHand-A. The main components shown include the driving tendons (in red), antagonistic tendons (in blue), differential mechanism due to the tendon layouts and couplings, driving and antagonistic motors, phalanges and tactile fingertips.

accuracy, as the behavior of passive components depends on their pre-set strengths and shapes, which may not suffice for intricate movements. Moreover, unlike motors, passive components cannot adjust their output characteristics, such as force and response speed, via software. In comparison, some robot hands based on a linkage drive excel in finger repeat positioning accuracy and response speed (Nurpeissova et al. (2021)). Nevertheless, they lack adaptability to various object shapes, a challenge that underactuated tendon-driven robotic hands can address (Catalano et al. (2014)).

Alongside the design and fabrication of the anthropomorphic hand, is its capability to be controlled, either autonomously or through human teleoperation. In this respect, having tactile sensing capabilities in the fingertips, and possibly over the rest of the hand, is necessary to provide direct information about contact. Historically, there have been many ways of integrating tactile fingertips into robot hands (Kappassov et al. (2015)); however, recently optical tactile sensors using cameras (Ward-Cherrier et al. (2018), Yuan et al. (2017)) have become prominent for various reasons, including the recent miniaturisation and cost-reduction in camera technology and the high-resolution nature of the sensory data fitting well with advances in computer vision. However, optical tactile sensors encounter bulky designs, making it difficult to integrate the component modules within the fingertip. Additionally, the complexity of the manufacturing process is another factor limiting the development of optical tactile sensors. Many such sensors, like DIGIT (Lambeta et al. (2020)) and 9DTact (Lin et al. (2023)), require specific molds and the casting of silicone to create soft skins. Others, like TacTip (Lepora (2021)), have

involved injecting gel fillers into skin cavities. These manual manufacturing processes significantly restrict the shape design of optical tactile sensors, as well as the variety and distribution of inner structures such as markers. Furthermore, the manufacturing errors inherent in manual production can further impact the generalization performance of optical tactile sensors based on deep neural network methods.

This paper explores the design and development of an antagonist tendon mechanisms coupled with fully-integrated 3D-printed tactile sensors that together enhance the functionality of highly-underactuated anthropomorphic robotic hands. One significant advantage we find is that by coordinating the drive motor and antagonistic motor, it is possible to actively control the distal interphalangeal (DIP) or proximal interphalangeal (PIP) joints of the fingers, which can be coupled with the tactile sensing to thereby effectively control grasp gestures while maintaining the hand's adaptive grasping. Another benefit is that active antagonism, by eliminating passive elastic elements, offers lower resistance during the hand-closing process, thereby increasing efficiency, responsiveness, and gripping strength.

Our **main contributions** in this work are:

- 1) We propose three different novel fingers with different antagonistic tendon mechanisms coupled with limited use of passive elastic components, which can achieve active control of the DIP and PIP joints respectively by using coordinating control of driving and antagonistic tendon.
- 2) We develop a fully 3D-printed tactile fingertip: utilizing advanced printing technology, we create multi-material and multi-hardness components in a single piece, eliminating the need for additional fabrication steps. Additionally, we

developed a simple tactile model capable of detecting contact and slip. We are the first to introduce this fabrication because of a novel 3D-printing step we introduce that mixes clear support material with other materials to adjust their softness. 3) We build a novel, underactuated robot hand with antagonistic tendon, tactile fingertips and new differential mechanisms. We also developed a control scheme that integrates tactile sensing with the antagonistic tendon mechanism to optimize the functionality of this hand: the Tactile SoftHand-A, named because of its inspiration from the Pisa/IIT SoftHand (Catalano et al. (2014)). Its performance, including adaptability and grasping ability, is evaluated through finger and hand-synergy experiments, and tactile-controlled grasping experiments.

This paper is organized as follows: Section II briefly describes and compares several representative underactuated robotic hands, highlighting their main features and differences from the Tactile SoftHand-A; additionally, some works related to vision-based tactile sensors are introduced. Section III details the design of our novel fingers equipped with various antagonistic tendon mechanisms. Additionally, we introduce a physical model to elucidate the working principle and include relevant workspace simulations. Section IV describes the design and development of the TacTip fingertip, detailing the tactile model for detecting contact and slip. Section V discusses the development of the Tactile SoftHand-A based on the D-type finger design where the DIP joint is controllable. This section covers the overall design, differential mechanism, and tendon layout. Section VI details the control scheme of Tactile SoftHand-A. Sections VII and VIII introduce the experimental design and results, respectively. Discussion of the results and conclusions is presented in Sections IX and X.

Background and Related work

Tendon-driven Robot Hand

At present, research on robotic hands has two main directions. One is to try to obtain the full dexterity of the human hand; *i.e.* to achieve all human hand functions by near-fully actuating the hand (Mohd Faudzi et al. (2018); Jacobsen et al. (1986); Butterfaß et al. (2001); Liow et al. (2019); Wang et al. (2019); Stuart et al. (2017)). The other direction is to reduce the complexity and control difficulty of robotic hands through tendon-driven (Chen et al. (2018); Li et al. (2022); Catalano et al. (2014); Mizushima et al. (2018)), pneumatic-driven (Zhu et al. (2023)) and linkage mechanisms (Kim et al. (2020)). This second approach benefits from progress in soft robotics, where there is morphological intelligence instantiated in the design and coupling of the structure comprising the hand.

Some near fully-actuated robotic hands seek to achieve complete dexterity, including the Shadow anthropomorphic hand, the UTAH-HIT hand (Jacobsen et al. (1986)) and the ROBISS hand (Mnyusiwalla et al. (2016)). The challenge with these hands is the complexity of the control needed to deploy the hand to grasp or manipulate objects and to operate the hand without damaging it.

The Pisa/IIT SoftHand (Catalano et al. (2014)) is inspired by the form of the human hand, but seeks to simplify the control by using just one tendon through all joints that is

driven by one actuator. This coupling between the elements of the hand gives it the ability to adapt to the shape of various objects. In addition, it uses a novel differential mechanism as an ingenious way to reduce the number of actuators while still having naturalistic hand movements that are characteristic of human hand motion (Sun et al. (2021); Xiong et al. (2016); Bicchi et al. (2011); Santello et al. (2016)). These differential mechanisms usually use the parallel slider mechanism (Sun et al. (2021)), moving-pulley mechanism (Gosselin et al. (2008); Gao et al. (2021); Chen et al. (2014)) or spring groups (Li et al. (2022)), which can be used to compose the synergy scheme (Catalano et al. (2014); Ozawa et al. (2014); Bicchi et al. (2011); Fan et al. (2018)).

In the process of studying the above robot hands, we found that almost all of the underactuated tendon-driven hands use passive elements such as torsion springs (Mnyusiwalla et al. (2016); Li et al. (2017); Jiang et al. (2014); Mizushima et al. (2018)), high-strength springs (Makino et al. (2017); Martin and Grossard (2014); Stuart et al. (2017)) and elastic bands (Catalano et al. (2014); Li et al. (2022); Ma and Dollar (2017); Stuart et al. (2017)) to achieve joint reset motion. Few underactuated tendon-driven hands use active extension to reset the fingers. Of these, one has proposed a robotic finger with release tendon and grasp tendon (Crisman et al. (1996)). However, its bearing and tendon layout limits the rotation angle of its finger joint since the tendon can detach from the bearing or axis during rotation, so its motion space is relatively small (Crisman et al. (1996); Lee et al. (1994)). Here we use a different bearing layout to guide the flexion tendon and extension tendon to increase the joint rotation angle of the joint. Another study proposed a robotic finger based on the biomimetics of human finger muscles, with two actuators for the adductive motion of the joints and control of the extension of the finger through a third actuator (Shirafuji et al. (2014)). However, that finger has a complex tendon layout that is not conducive to the design and assembly of the overall hand. Furthermore, we have observed that currently, no tendon-driven robotic hand can decouple the DIP or PIP joint while ensuring adaptive capability, nor actively control the DIP or PIP joints to adjust the grasping gesture while maintaining adaptive grasping ability.

Therefore, here we propose a novel tendon-driven finger design that achieves active extension and control of the DIP or PIP joints through coordinated control of driving and antagonistic tendons. Based on this new design, we have also developed a novel robotic hand that with just two motors can actively-manage closing, opening and grasping gestures.

Vision-based Tactile Sensing

Compared to piezoelectric and resistive sensors, vision-based tactile sensors (VBTS) are increasingly favored by robotics experts due to their superior spatial resolution, which provides richer physical information for robotic interaction tasks, such as texture features and object pose. Researchers have developed many VBTS, such as MIT's Gelsight (Yuan et al. (2017)), META's DIGIT (Lambeta et al. (2020)), BRL's TacTip (Ward-Cherrier et al. (2018), Lepora (2021)) and BioTacTip (Li et al. (2024)). However, the manufacturing processes for these sensors are complex and labor-intensive, typically exceeding five hours. For instance, creating the DIGIT involves using specialized molds for

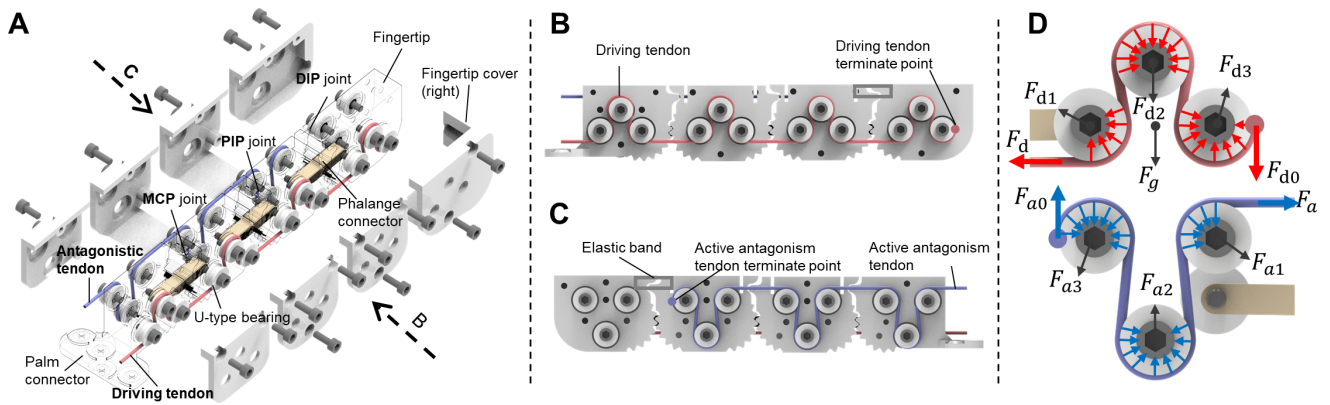


Figure 2. The D-type finger where the antagonistic tendon terminates on the DIP joint. (A) Exploded view. (B) Right view. (C) Left view. (D) Diagram showing the forces for analysis of the motion of the D-type fingertip.

silicone casting to form its soft skin. Also, the use of transparent windows in all VBTSs mentioned above requires laser equipment for cutting and hand-placement/gluing the window. In manufacturing the TacTip and BioTacTip (Li et al. (2024)), transparent gel is injected into the skin and window cavities, and specialized vacuum equipment is necessary to remove any bubbles that may form during injection and curing. Furthermore, when integration with a robotic fingertip is needed, researchers must create new molds, and produce connection parts to the phalanges. Additionally, the manual production methods of VBTS, such as variations in silicone pouring and injection, lead to physical performance discrepancies among sensors, such as stiffness and sensor skin shape, which pose challenges in generalizing models trained on individual sensors in practical applications.

Therefore, we have developed a new printing technology that allows for the 3D printing of multi-material and multi-component parts without any post-fabrication steps such as gel injection or glue windows. Using this technology, we have for the first time integrated VBTS with the phalanges of a robotic hand in a single print.

Development of Robot Fingers Featuring Active Antagonism

Based on different tendon configurations, we have developed three types of fingers, each exhibiting distinct flexion gestures, termed the A-type finger, D-type finger and P-type finger, respectively (for antagonistic, distal and proximal). The A-type finger, which features an antagonistic tendon running through the entire finger, exhibits the fastest extension. The D-type finger features active control of the distal interphalangeal (DIP) joint, achieved through the coordination of a driving tendon and an antagonistic tendon and a passive element on the DIP joint. Similarly, the P-type finger employs a comparable mechanism to actively control the proximal interphalangeal (PIP) joint. Their design details are as follows.

Design of A-type finger

In contrast to the D-type and P-type fingers, the antagonistic tendon of the A-type finger terminates at the fingertip (Figure 3(A)). This means that the A-type finger does not require an elastic band or other passive element to

assist with its extension, resulting in a simpler structure. Consequently, during finger flexion, the absence of resistance from an elastic band leads to greater fingertip force and faster reactions compared to the other two types of fingers. However, despite these advantages, the A-type finger lacks active control capabilities for the DIP or PIP joints, unlike the other two types, the effect of which will be assessed experimentally.

Design of D-type finger

As illustrated in Figure 2(A), the D-type finger primarily consists of phalanges, phalangeal coverings, tendons, and a bearing mechanism. Its total length, width, and height are 115 mm, 20 mm, and 23 mm, respectively. The phalanges are composed of a fingertip, two middle phalanges, and a base phalanx, interconnected through gear engagement to form three rotary joints: the Distal Interphalangeal (DIP), Proximal Interphalangeal (PIP), and Metacarpophalangeal (MCP) joints. A bearing mechanism with multiple U-type grooves is also affixed to the four phalanges. The driving tendon (Figure 2(A), red cable) and antagonistic tendon (Figure 2(A), blue cable) run through the entire finger via the U-type grooves on the bearings. For instance, bearings arranged in an equilateral triangle on the right side of the middle phalanx facilitate flexion movement by providing driving force to the driving tendon. Conversely, bearings in an inverted triangle arrangement on the left side support extension movement. Notably, the antagonistic tendon of the D-type finger terminates at the first middle phalanx. Therefore, the force required for resetting the DIP joint is provided by an elastic band positioned between the fingertip and the first middle phalanx, coupled to the active reset of the other finger joints.

Design of P-type finger

The primary structure of the P-type finger is identical to that of the D-type finger. The only difference lies in the configuration of the antagonistic tendon (see Figure 3). Unlike the D-type finger, the antagonistic tendon of the P-type finger terminates at the second middle phalanx. Consequently, it is necessary to incorporate passive components at the DIP and PIP joints to facilitate the

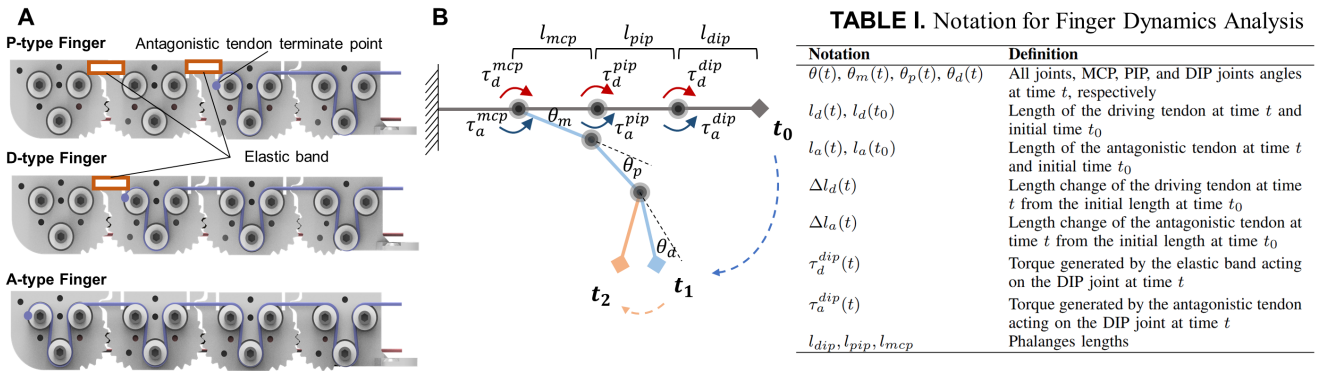
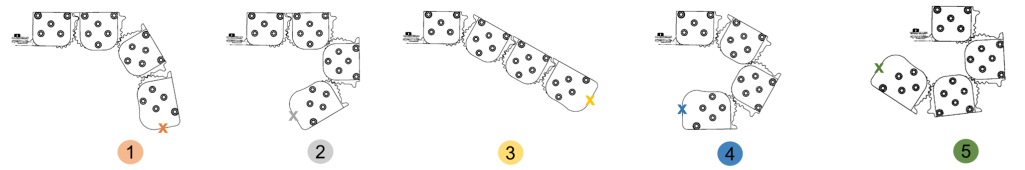
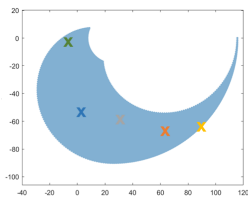
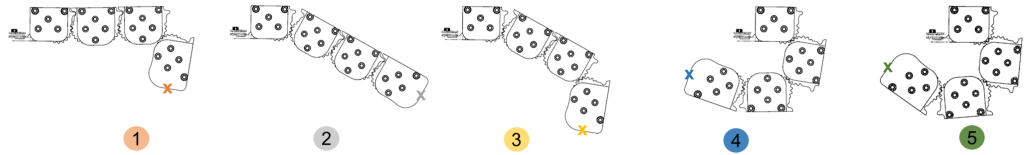
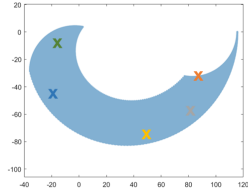


Figure 3. Antagonistic tendon comparison for P-type, D-type and A-type fingers. (A) Side view of three type fingers. (B) Schematic model of all fingers showing the main variables of interest (described in TABLE I).

(a) P-Type Finger Workspace



(b) D-Type Finger Workspace



(c) A-Type Finger Workspace

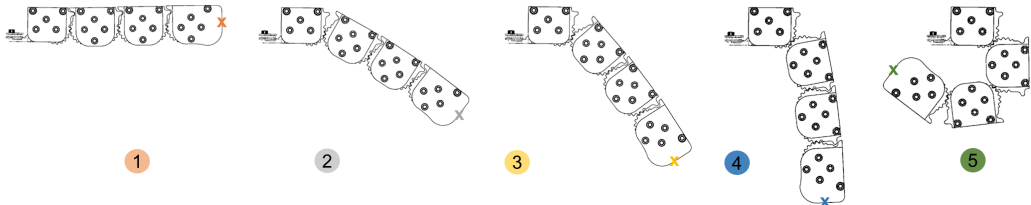
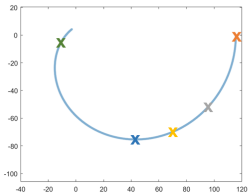


Figure 4. Workspace comparison of the P-type, D-type and A-type fingers. The left shaded regions show the entire workspaces for the tip of the fingers, with illustrative finger shapes within those workspaces shown to the right. Note the larger workspaces of the P-type and D-type fingers due to the capability to control the PIP and DIP joints, compared to that of the A-type finger.

repositioning of the corresponding phalanges, where we use elastic bands similar to the D-type finger.

Dynamics Analysis of D-type Finger

This section primarily analyzes how to achieve control of the DIP joints of the fingers at any position through coordinated control of the driving tendons and antagonistic tendons. Several methods exist for modeling the dynamics of tendons, including particle models, continuum models, and rigid body models. However, for the Tactile SoftHand-A, which features ten tendons connected by differential mechanisms and passive components, such models become overly complex and difficult to integrate with control systems. Therefore, we adopt an analytic model in which the force distribution and the schematic of the finger are shown in Figures 2(D) and 3(B) respectively. The meaning of all notation for finger dynamics analysis are introduced in TABLE I. The meanings of all notations used for finger dynamics analysis

are presented in TABLE I. There are two periods that describe the movement of the D-type finger: one without active control of the DIP joint from time t_0 to t_1 , and another with active control of the DIP joint from t_1 to t_2 .

The finger rotation angle $\theta(t)$ is given by the sum of DIP rotation angle $\theta_d(t)$, PIP rotation angle $\theta_p(t)$ and MCP rotation angle $\theta_m(t)$:

$$\theta(t) = \theta_m(t) + \theta_p(t) + \theta_d(t). \quad (1)$$

The change of driving tendon and antagonistic tendon can be represented by $\Delta l_d(t)$ and $\Delta l_a(t)$, where

$$\Delta l_d(t) = |l_d(t) + l_d(t_0)|, \quad (2)$$

$$\Delta l_a(t) = |l_a(t) + l_a(t_0)|. \quad (3)$$

First, we consider a period from t_0 to t_1 , in which the active antagonism synchronizes with the driving tendon.

Therefore, there is no resistance acted on MCP and PIP joint:

$$\tau_{m.a}(t_1) = \tau_{p.a}(t_1) = 0, \quad (4)$$

$$\begin{aligned} \Delta l_d(t_1) &= \Delta l_a(t_1) = \theta(t_1) \cdot l \\ &= \theta_m(t_1) \cdot l_3 + \theta_p(t_1) \cdot l_2 + \theta_d(t_1) \cdot l_1. \end{aligned} \quad (5)$$

Now, in a second period from t_1 to t_2 , we use active antagonism to control the DIP joint. We keep the active antagonism at the same length and pull the driving tendon:

$$\Delta l_a(t_2) = \Delta l_a(t_1), \quad \tau_{m.a}(t_2) = \tau_{p.a}(t_2) = \infty. \quad (6)$$

Therefore, the difference in tendon lengths between the driving and antagonistic tendon is

$$\begin{aligned} \Delta l_d(t_2) - \Delta l_a(t_2) &= \Delta l_d(t_2) - \Delta l_a(t_1) \\ &= (\theta_d(t_2) - \theta_d(t_1)) \cdot l_1, \end{aligned} \quad (7)$$

which results in bending of the DIP joint.

Therefore, we can actively control the DIP joint by controlling the displacement of driving tendon and active antagonistic tendon.

Comparisons of Finger Workspace in Simulation

After demonstrating that A-type, D-type and P-type fingers can execute diverse gestures through the coordinated control of driving and antagonistic tendons, an important comparison is their workspaces. To this end, we utilized the MATLAB Robotics Toolbox to construct models for these finger types, employing the Denavit-Hartenberg (DH) matrix to evaluate their workspaces. For example, the D-type finger, requires an independent control input for active management of its DIP joint due to its capability for autonomous movement; meanwhile, the proximal PIP and MCP joints are interconnected, necessitating a separate control input to adjust the angles of both PIP and MCP joints. By applying the Monte Carlo method to generate varied inputs, we employ forward kinematics to delineate the fingertip's workspace (Figure 4).

Using the above method, we plotted the fingertip vertex positions for various gestures in the simulator (Figure 4). Unlike the D-type and P-type fingers, A-type fingers lack active control over the DIP or PIP joints, resulting in a workspace confined to a fixed arc due to the coordinated action of driving and active antagonistic tendons (Figure 4(c)). Notably, the D-type finger demonstrates a more uniform workspace distribution, particularly in extended gestures, leading to the selection of D-type configured fingers for testing and developing the Tactile SoftHand-A, as discussed in the later sections of this paper.

It is worth noting that the above simulation was completed without touching any objects or obstacles; because the fingers have adaptive capabilities, simulating workspace changes in contact with objects or obstacles are not discussed in this section, but instead are evaluated experimentally later.

Development of fully-integrated tactile fingertips

The fingers are intended to have optical tactile sensing in the distal phalanges. Here we introduce a novel design where

the entire sensing structure of the fingertip is 3D-printed as a single component integrated into the physical structure of the finger, requiring no manual fabrication except for the insertion of the camera module. First, we detail the main components and design considerations of the fully-integrated fingertips, then their fabrication utilizing advances in multi-material 3D-printing technology.

Integrated tactile fingertip design

As depicted in Figure 5, the tactile fingertip comprises three modules: the perception module, the contact module, and the actuation module. The perception module is composed of a camera and an LED strip: the camera captures high spatial resolution tactile images, while the LED strip mounted on the front of the tactile fingertip skeleton provides consistent lighting inside the contact module. The actuation module, consisting of bearings and a tendon mechanism installed on either side of the tactile fingertip skeleton, provides torque for fingertip rotation. The contact module components include the fingertip skeleton, a clear window, window cover, soft transparent filling material, markers, and the skin surface. The fingertip skeleton integrates a gear match area to form a gear pair with the second phalanx.

The perception and actuation modules are also mounted on the phalangeal skeleton, with bearings and the tendon mechanism secured by bolts on both sides. The camera lens and camera board are affixed to the top of the fingertip. The skin surface, located at the fingertip's pad, converts external contacts into internal deformation, thereby moving markers attached on pins to its inner surface based on the TacTip design (Ward-Cherrier et al. (2018)). These are then captured by the camera to form tactile images. Additionally, the black outer skin surface and window cover isolate external light interference, to aid producing high-quality tactile images. The soft, transparent clear fill is designed to increase the surface's deformation range while providing internal support and resetting its deformation. The rigid, transparent clear window serves to support the clear fill and refract light from the LED strip.

Fabrication of the tactile fingertip

The perception and actuation module components of the tactile fingertip can be purchased inexpensively, while the remaining components are all produced using multimaterial 3D-printing (Stratasys J826). The entire assembly of the contact module's components, including the soft black opaque surface (soft agilus material), hard white markers (hard verowhite material), soft transparent filling (soft agilus clear mixed with support material), hard transparent window (hard veroclear material), hard black opaque window cover, and the hard white skeleton (hard verowhite material), are integrally formed as a single component without any other post-fabrication processes required.

The new capability to 3D-print the assembly of the contact module as one piece offers significant benefits in ease of assembly and fabrication repeatability. In previous versions of the TacTip (Lepora (2021)), after printing we needed to clean the support, glue the acrylic window, inject gel (requiring mixing then degassing in a vacuum chamber), then leave in a dryer for 10 hours or more before it could be used.

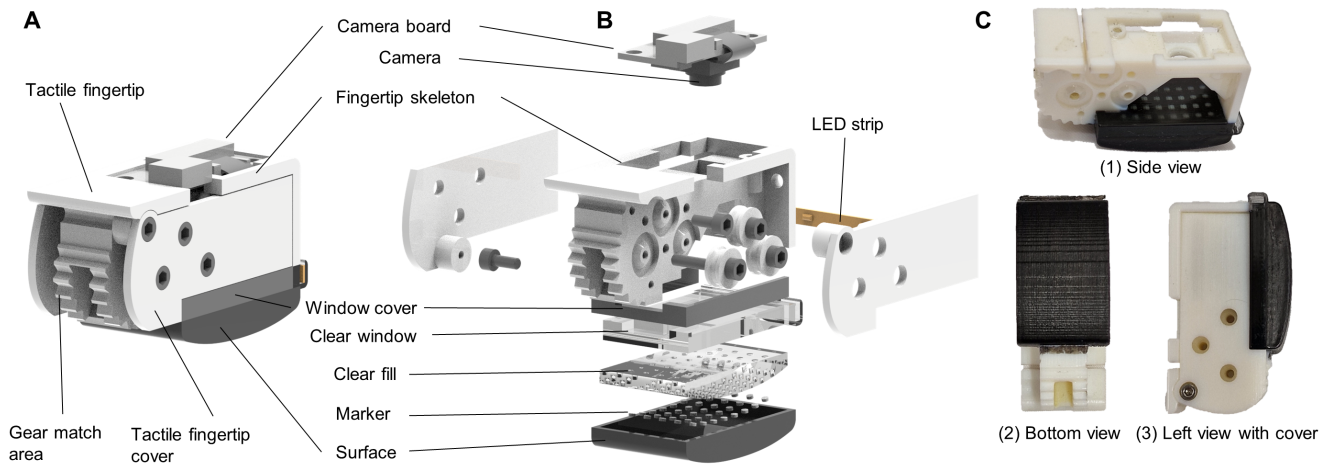


Figure 5. Construction and design of the fully 3D-printed tactile fingertip. (A) side view. (B) Exploded view. (C) Print and construction of the tactile fingertip. The only hand fabrication is to insert the camera board in the top on the fingertip.

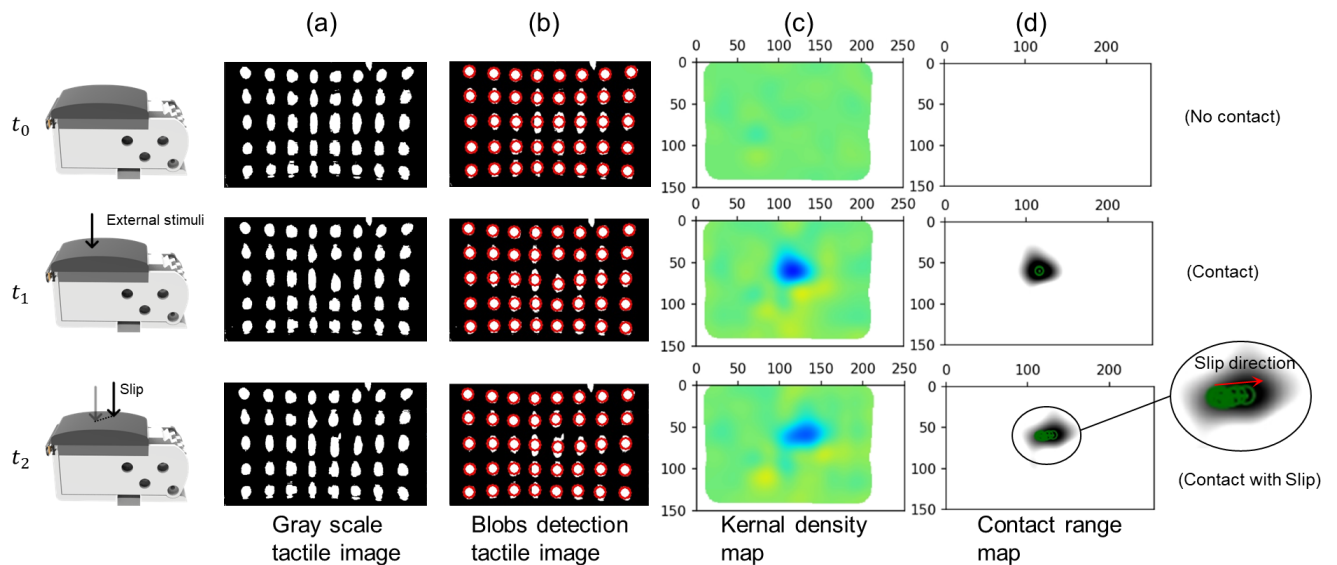


Figure 6. Tactile image processing under contact and slip for three consecutive times t_i . (a) Raw grayscale tactile images. (b) Marker detection using the DoH blob-detection method (red circles). (c) Contact map by applying a Gaussian kernel density transformation on the marker centroids, with the contact region visible in blue. (d) Extracted contact centroid (middle row, green circle) and effect of contact slip (bottom row, green circles and red arrow).

By using this new technology, we can quickly produce tactile fingertips, from design to application in just 1 hour.

This capability is made possible by an innovation we have introduced in mixing support material with Agilus material to print a clear fill that, while maintaining its transparency, can have its hardness adjusted by altering the proportion of support material. Previously, the hardness of the pure Agilus material available with the printer was found to be excessively high for use as a soft filler. Usually, the support material is required for the layering of complex structures and is cleaned post-printing. Fortunately, one of the support materials happens to be optically clear and we found it is compatible with mixing with other materials, which lends it to adjusting the filling material's softness.

Tactile Localization Model

The camera images through the perception model are then processed with a corresponding tactile model (Figure 6).

Here we are primarily concerned with predicting and using the contact region and its centre point, which we will integrate into the robot hand control. The model details are described below.

Image Preprocessing: Initially, the image captured by the camera is cropped to the region in which markers are visible. Subsequently, binary processing is applied to the cropped image, using thresholding on the pixel intensity (set to 180 on a 0 to 255 scale). These preprocessing steps yield a binarized image I_{gray} in which the markers are clearly visible.

Marker Detection: We employ the Determinant of Hessian (DoH) estimation method for marker detection to identify white markers in images. The DoH estimation method is a widely-recognized technique in image processing and computer vision for its efficacy in identifying blob features. It operates by locating local maxima of the determinant of the Hessian matrix at every image point. For the given image

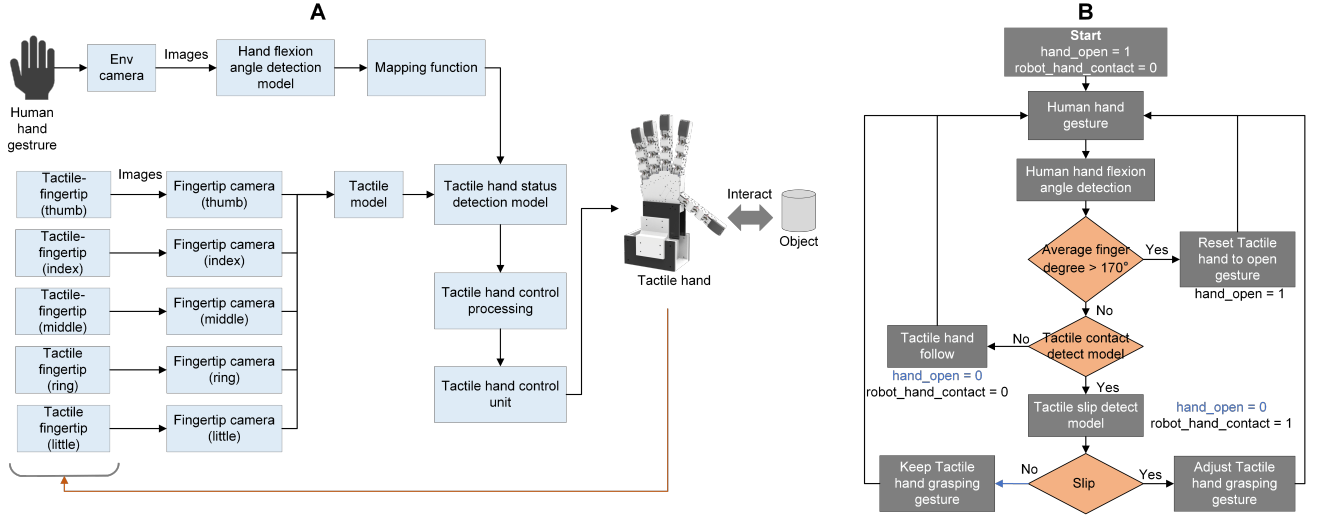


Figure 7. Schematic diagram for the processing modules and tactile feedback grasping control flow chart, which are used to control the hand both in open loop from human gestures and closed loop from the tactile feedback.

I_{gray_i} , the Hessian matrix at a point (x, y) is defined as:

$$H(\mathbf{x}) = \begin{bmatrix} L_{xx}(\mathbf{x}) & L_{xy}(\mathbf{x}) \\ L_{yx}(\mathbf{x}) & L_{yy}(\mathbf{x}) \end{bmatrix}, \quad (8)$$

where the components represents the second partial derivatives in the x and/or y directions. We note that a scale parameter σ is applied to perform Gaussian Kernel smoothing on the image prior to computing the matrix. This step aids in noise reduction and facilitates feature detection across different scales. Marker detection is achieved by identifying the locations in the image where the Hessian matrix attains a local maximum. The positions of these markers are denoted by (x_m, y_m) .

Contact Region Estimation: Markers within the contact region are influenced by external contacts, levering them towards adjacent uncontacted regions, thereby diminishing the marker density in the region of contact. Consequently, the location of the contact region can be inferred by analyzing the local marker density. Here we adopt an methodology involves the following steps: upon identifying the markers, we compute the marker density using a Gaussian kernel density estimation method. This approach positions Gaussian kernels at the marker centroids, with a constant kernel width h determined by the mean distance between neighboring markers:

$$\bar{d}(x, y) = \frac{1}{M} \sum_{m=1}^M \frac{1}{\sqrt{2\pi}h^2} \exp\left(-\frac{\|(x, y) - (x_m, y_m)\|^2}{2h^2}\right), \quad (9)$$

where the square-distance norm $\|(x, y) - (x_m, y_m)\|^2 = (x - x_m)^2 + (y - y_m)^2$. We can see from Figure 6(c) that the extent of the low marker density areas in the kernel density map (blue region) depends on the contact depth and reflects the contact area. Finally, we calculate the lowest density point within that region to find the center of contact area ($R_c(x_c, y_c)$).

$$R_c(x_c, y_c) = \arg \min_{(x, y) \in \mathbb{R}} \bar{d}(x, y). \quad (10)$$

As shown in Figure 6(d), this represents the contact center (shown as a green circle).

Development of the Tactile SoftHand-A

Overall Design

The Tactile SoftHand-A is a major advancement over the previous design of the BPI-SoftHand (Li et al. (2022)), with its use of novel D-type fingers featuring active antagonism, coupled with a modified two-layer palm design for distinct routing of driving and antagonistic tendons, and utilization of two differential mechanisms (Figure 1). We previously introduced three different types of novel fingers; the D-type fingers were selected for their more evenly distributed workspace and used in constructing the Tactile SoftHand-A. Overall, the hand has 15 degrees of freedom and 2 degrees of actuation, with each finger encompassing three joints: MCP, PIP, and DIP, marking an evolution in design and functionality from the previous BPI SoftHand. The overall length of Tactile SoftHand-A is 200 mm with palm width 90 mm and length 26 mm from palm to back cover.

The parts of each finger are depicted in the exploded design illustrations in Figure 2. The hand employs two distinct tendon schemes for the operation of the fingers: one for flexing and another for extending. This dual-tendon system features a soft synergy mechanism, linking each of the five tendons via a spring to its coupling mechanism (tendon spool) and to the differential mechanism, which then connects to a shared spool on the motor, ensuring a coordinated and smooth motion.

Differential Mechanism

The Tactile SoftHand-A has two differential mechanisms: one for the active flexing movement of the fingers and one for the active antagonistic movement of the fingers. Each differential mechanism consists of a soft synergy scheme that couples the tendons for flexion and extension separately to springs, with each mechanism connected to a separate tendon coupling driven by a servo motor (see Figure 1). Through

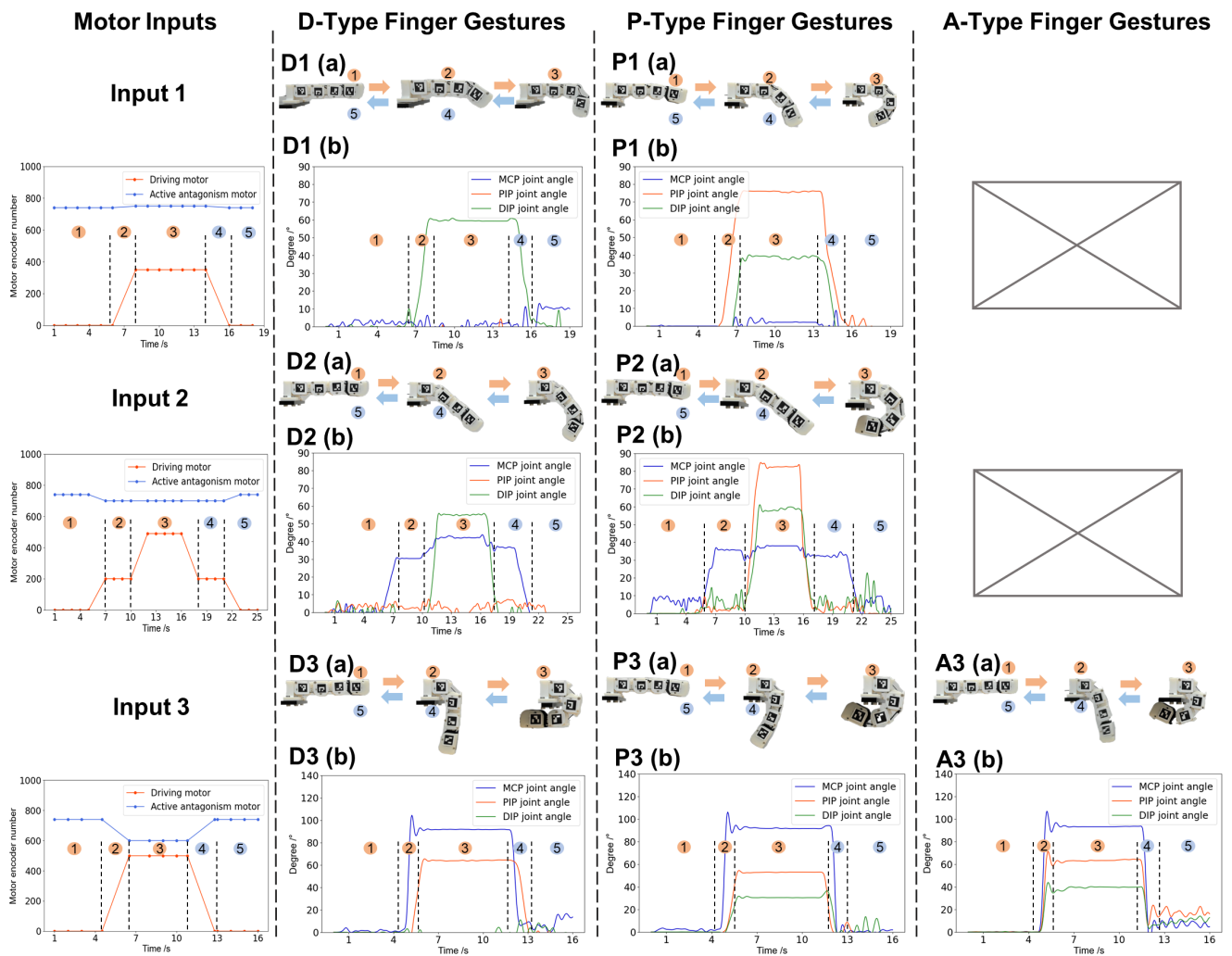


Figure 8. Gestures for the D-type, P-type and A-type fingers under different control inputs to the driving and antagonistic motors (motor inputs 1 to 3, shown to left). The corresponding angles of the MCP, PIP and DIP joints in real time are shown to the right (plots D1-D3 for D-type; P1-P3 for P-type and just A3 for A-type). The A-type finger does not have the ability to move under inputs 1 and 2 due to the absence of soft elements, so there are no plots for A1 and A2. The results in this figure relate to Experiment A.

the combined differential mechanism, the entire hand can be actively opened and closed with two motors. Hence, the synchronization of all fingers can be achieved easily, and grasping adaptability is also kept, as will be verified in the experimental results.

Palm Tendon Layout

To mitigate friction during tendon force transmission, bearing groups were strategically positioned within the palm, as shown in Figure 1(B). The setup for the index finger's antagonistic tendon illustrates this approach: a bearing set guides the tendon at the finger's base, preventing direct contact with the base phalanx cover. This arrangement ensures the tendon follows a defined path to the bottom of the palm, where it connects to the guiding mechanism and subsequently to a spring, thus avoiding palm contact and minimizing friction during operation.

Human-guided Control Scheme

When not in contact with an object, using the robotic hand to mirror human hand gestures simplifies control complexity (Gioioso et al. (2013)). Upon contact, the robotic

hand can effectively utilize tactile feedback information to automatically adjust its grasping gestures, thereby enhancing its grasping capability. To achieve these objectives, we have developed a tactile feedback control system for Tactile SoftHand-A. It is comprised of four main components (Figure 7): human hand gestures, a PC, a motor controller, and the Tactile SoftHand-A. It operates by translating various hand gestures into control commands. The PC processes raw images of human hands captured by an external camera, along with tactile images from the fingertips of the Tactile SoftHand-A. These images are then converted using the gesture and tactile models into motor control parameters, which are transmitted to the motor controller using UART serial communication. The motor controller primarily utilizes PID control to adjust the rotation of two servo motors, thereby enabling the Tactile SoftHand-A to interact with its surroundings.

Open-loop Control Strategy

In experiment A, we use 3 different constant inputs for motors to control P-type, D-type and A-type fingers. By observing the varying gestures of these three types of fingers

under the same motor input, we can evaluate the effect of different antagonistic tendon layouts on finger gestures. In Experiments B and C, we implemented an open-loop control strategy without tactile feedback to emphasize the Tactile SoftHand-A's adaptability to objects' shape and its capability for varied grasping gestures. Of note, experiment B employed fixed motor inputs to regulate the grasping mechanism of the Tactile SoftHand-A, intentionally reducing the impact of human intervention to underscore its inherent mechanical intelligence. For experiment C, we employed a variety of motor inputs by modifying the encoder difference between the driving and antagonistic motors, demonstrating the Tactile SoftHand-A's versatility in performing a range of grasping gestures.

Closed-loop Control Strategy

In addition, we developed a tactile feedback grasping control system that integrates tactile and antagonistic tendon mechanisms to adjust the Tactile SoftHand-A's grasp gestures via tactile feedback, preventing objects from slipping. Figure 7(A) provides a schematic diagram of the system, while Figure 7(B) illustrates the control flow chart. The system architecture employs a multi-processing approach, as described next. An environmental camera captures real-time images of the human hand, extracts joint landmark points using Mediapipe, and calculates the angles between the fingers and palm. When the tactile sensors in the Tactile SoftHand fingertips do not detect contact, the Tactile SoftHand-A synchronizes with human hand gestures by converting angles into motor inputs through a mapping function. Upon detecting contact, the system switches to tactile feedback closed-loop control, and Tactile SoftHand-A stops synchronizing human hand gestures. The tactile model then checks for slippage by determining if the displacement of the contact point exceeds a threshold. If no slippage is detected, Tactile SoftHand-A maintains the current grasp. If slippage is detected, Tactile SoftHand-A adjusts the grasp gesture and rotates the DIP joints inward to apply greater normal force, preventing the object from slipping. To release an object or grasp a new one, the human hand must be fully opened (with an average angle between the fingers and palm greater than 170 degrees) to exit the tactile feedback closed-loop control. The tactile SoftHand-A will then resynchronize to the human hand gestures until the next contact.

Experiments

Experiment A - Finger Gestures Comparison

In this finger experiment, we verify the respective controllability of the DIP and PIP joints of the D-type and P-type fingers, by demonstrating how coordinated control of the driving tendon and antagonistic tendon enables active control of the appropriate joints. The A-type finger, due to its antagonistic tendon layout, cannot decouple joints and is used for comparison with other types of fingers. For the D-type, P-type and A-type fingers, Aruco marker codes attached to the phalanges' sides record the angular changes of the DIP, PIP, and MCP joints, which are then displayed in line graph form (Figure 8). Correspondingly, the input to

the motors (encoder values) is also represented in line graphs (Figure 8, motor inputs).

Experiment B - Controllable Grasping Gestures

In this hand experiment, we illustrate the capability of the Tactile SoftHand-A to perform controllable grasping gestures. By adjusting the input difference between the driving motor and the antagonistic motor (Figure 9A), we can precisely control the grasping gestures. The behaviour of the hand, displaying both the front and side views under various inputs, is presented in Figure 9B.

Experiment C - Grasping Adaptability

This experiment demonstrates the object-shape adaptation ability of the hand. The Tactile SoftHand-A was mounted on the experimental bench, with fixed motor inputs controlled by the driving and antagonistic motors, enabling the Tactile SoftHand-A to grasp various objects (for the types of motor inputs shown in Figure 10(C)). We selected three objects with constant cross-sections: a hexagonal prism, a triangular prism, and a cylinder; and two multi-section objects: a wine glass and a tendon spool (all objects shown in Figure 10(A)). The single-section objects have a uniform volume and are of height 76 mm, whereas the wine glass and tendon spool measure 136 mm and 89 mm in height, respectively. This setup allowed evaluation of the SoftHand's adaptability to different objects by comparing the contact conditions of each joint during the grasp. Statistically, we adopted two metrics to assess performance: the average number of contacted fingertips assessed from the tactile sensing, and the proportion of successful grasps (assessed over 10 grasps for each object, varying the placement of the object in hand).

Experiment D - Tactile Feedback Control

To evaluate the performance of the tactile feedback control system described (shown in Figure 7), we designed an experiment aimed at demonstrating its capabilities in slip detection and adjusting grasping gestures with tactile feedback. We employed human hands for contact testing, specifically using the thumb tactile sensor of the Tactile SoftHand-A. The experiment is structured into three sequential stages: synchronization, contact and slip. In the synchronization stage, the Tactile SoftHand-A aligns with the gestures of the human hand. During the contact and slip stages, the system engages in closed-loop tactile feedback control. In the slip stage, we assess the system's ability to detect slip and modify grasping gestures by artificially inducing slip to the thumb of the Tactile SoftHand-A. The results are shown in Figure 13.

Results

Results A - Finger Gestures Comparison

We use the D-type finger as an example to illustrate the active control of the DIP joint through coordinated control of the driving and antagonistic motors. Initially, in the finger extension state, the driving motor is position-controlled to rotate a specific angle, pulling the driving tendon and generating a driving force on the finger. Concurrently, the active antagonism is position-controlled to slightly reverse,

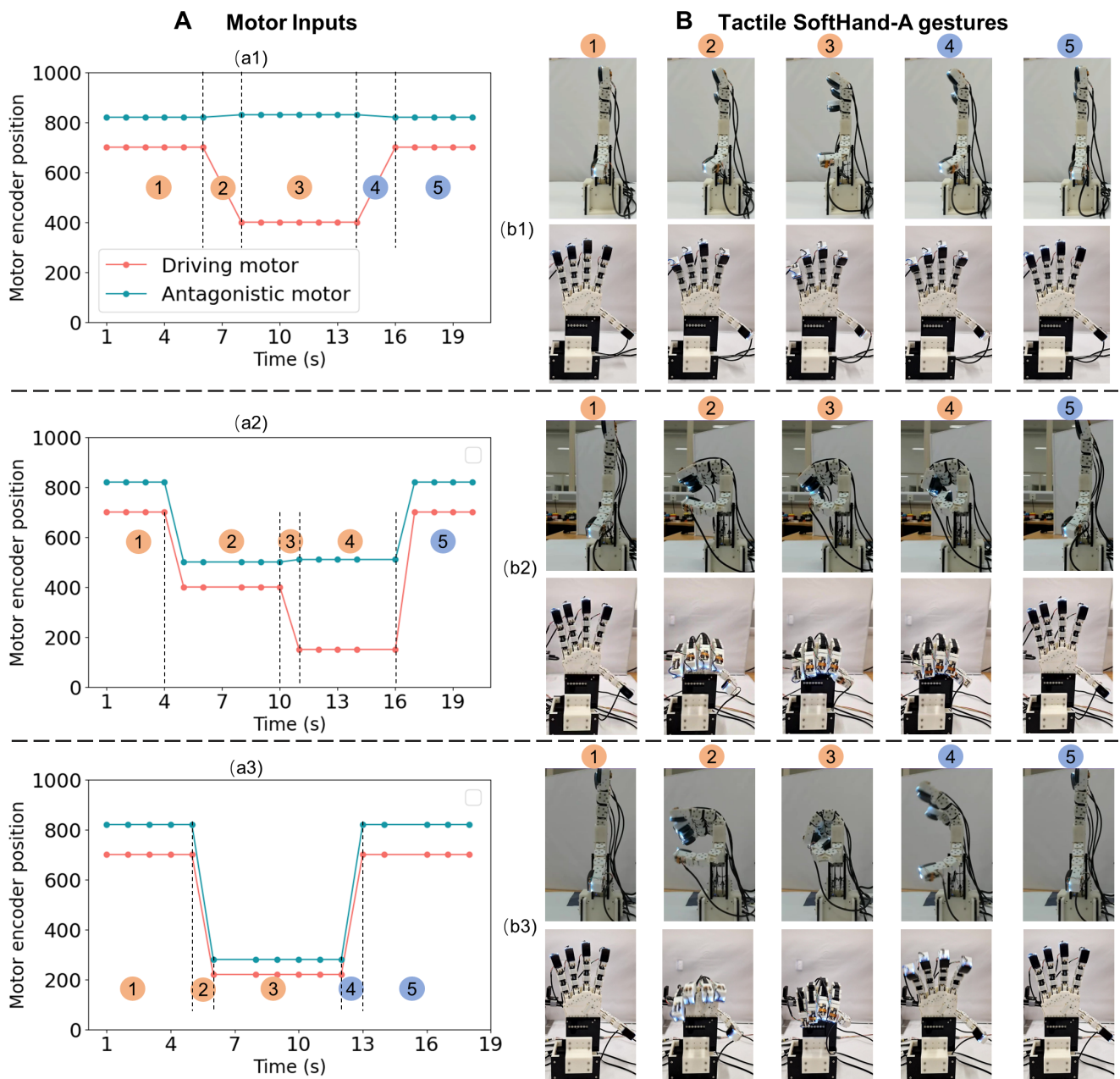


Figure 9. Response of the entire SoftHand-A with D-type fingers to different motor inputs. (A) The three examples of motor input are intended to show that, through the coordinated control of the driving motor and active antagonistic motor, SoftHand-A can achieve changes in grasping gestures through active control of all DIP joints. (B) SoftHand-A gesture changes under these inputs at different points in the trajectory. The red points are taken from the closing trajectory of the SoftHand-A, while the blue points are taken from the opening trajectory of the SoftHand-A. The results in this figure relate to Experiment B.

thus eliminating the slack in the tendon. As a result, substantial opposing forces are generated at the PIP and MCP joints. Due to the driving tendon passing through the entire finger and resistance at the MCP and PIP joints, active control of the DIP joint is achieved. Figure 8 D1(a) displays the gestures of the D-type finger in actual experiments. The green line in Figure 8 D1(b) represents the changing angle of the DIP, while Figure 8 Input 1 details the input changes to the driving and antagonistic motors in this procedure. Figure 8D1(a-b) shows the D-type finger achieving active control of the DIP in a semi-flexion state, following a similar control process. Figure 8D3(a-b) shows the D-type finger in full flexion. The control of the P-type and A-type fingers are similar to that of the D-type, with detailed results in Figure 8.

Results B - Controllable Grasping Gestures

As illustrated in Figure 9A(a), under the open hand gesture of the Tactile SoftHand-A, control over all fingers' DIP joints is achieved by increasing the differential between the driving motor and the antagonistic motor. Notably, in the initial phase, increasing the encoder of the antagonistic motor (to reverse its direction at phase 3) tightens the antagonistic tendon, thereby preventing the fingers' PIP and MCP joints from bending actively. The actual experiment's representations, including the front and side views of the Tactile SoftHand-A, are displayed in Figure 9B(d-e). Here, the bending of all fingers' DIP joints is distinctly observable as the motor differential increases, reaching its maximum at phase 3.

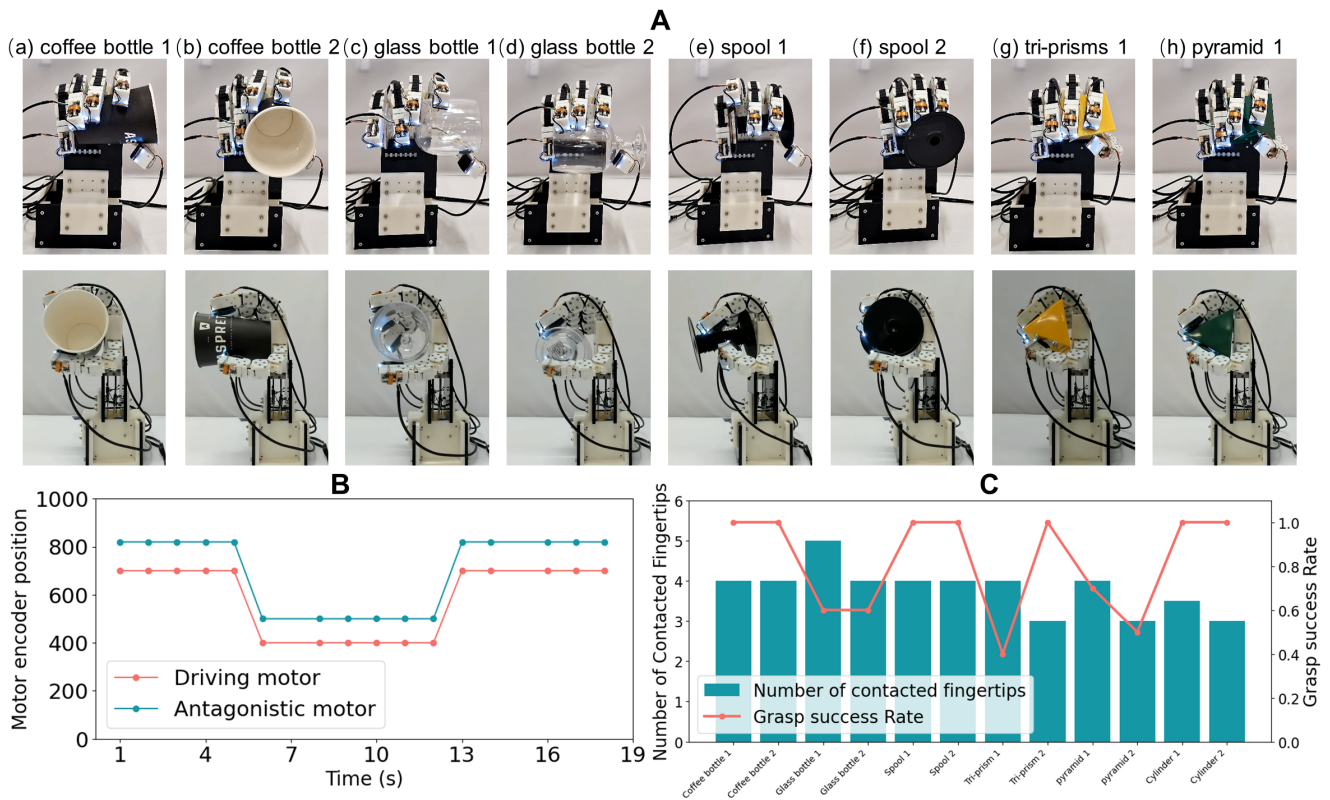


Figure 10. Grasping adaptability of the tactile SoftHand-A with D-type fingers to various objects with the same motor inputs. (A) Front and side views of the hand at maximal closure. (B) Motor input. (C) Grasp success rate and number of contacting fingertips (validated from the tactile outputs). The grasp success rate is calculated as the number of times an object is successfully grasped in ten grasping experiments. A successful grasp is when the object is grasped for more than 5 seconds under the influence of gravity. The results in this figure relate to Experiment C.

In Figure 9A(b), we first reduce the encoders of both the driving motor and the antagonistic motor simultaneously to coordinate their rotation (phase 1-2), and then increase the differential between them (phase 3-4). This enables active control of the DIP joints while the hand is in a semi-closed state. The corresponding actual presentations are depicted in Figure 9B(f-g). We observe that in phases 1-2, the Tactile SoftHand-A begins to close. Subsequently, in phase 3, active control over the rotation of the fingers' DIP joints commences, reaching its maximum in phase 4, followed by a return to an open position in phase 5.

By contrast, in Figure 9A(c), coordinating the rotation of the driving motor and the antagonistic motor without activating the active antagonism allows for the hand to close and open normally.

Results C - Grasping Adaptability

From Figures 10A and B, we observe the interaction between the Tactile SoftHand-A and the grasped objects. Specifically, Figure 10A(a) illustrates how the thumb, positioned opposite the other four fingers, forms an arc to effectively encircle and stabilize objects, enhancing grip support. This arrangement and differential mechanism allow the remaining fingers to flex to various extents, adapting to the object's shape and demonstrating the Tactile SoftHand-A's adaptability to different object contours.

In the case of grasping single-section objects include the hexagonal prism, triangular prism, and cylinder, the

fingers, upon making contact, permit the little finger to retract towards the palm, as depicted in Figure 10B(a-c). This flexibility is attributed to the novel differential mechanism, which is not limited to the little finger alone.

Furthermore, as shown in Figure 10A and B(d-e), when engaging with multi-section objects, each finger joint adjusts its bending to conform to the object's shape, showcasing the Tactile SoftHand-A's adaptability in grasping varied geometries. For example, after the little finger, thumb, and index finger of the Tactile SoftHand-A make contact with the outer flange of the tendon spool, the ring and middle fingers can still bend until they touch the central axis of the tendon spool.

Results D - Tactile Feedback Control

Figure 13 depicts various time points during the gesture synchronization phase (1-15 seconds), where 1 to 3 represent specific moments of synchronization stage. At this stage, Tactile SoftHand-A synchronizes with the gestures of the human hand. For instance, at time point 1, Figure 13(A) illustrates the human hand in an open position, while Figure 13(B) shows Tactile SoftHand-A in a similar fully open state. By time point 3, Figure 13(A) depicts the human hand partially closed, and the Tactile SoftHand-A mirroring this gesture in Figure 13(B). Figure 13(C)(2) demonstrates that the input curves of the two motors follow a similar trend to the finger angle curve of the human hand, showcasing effective synchronization of the human and robot hand

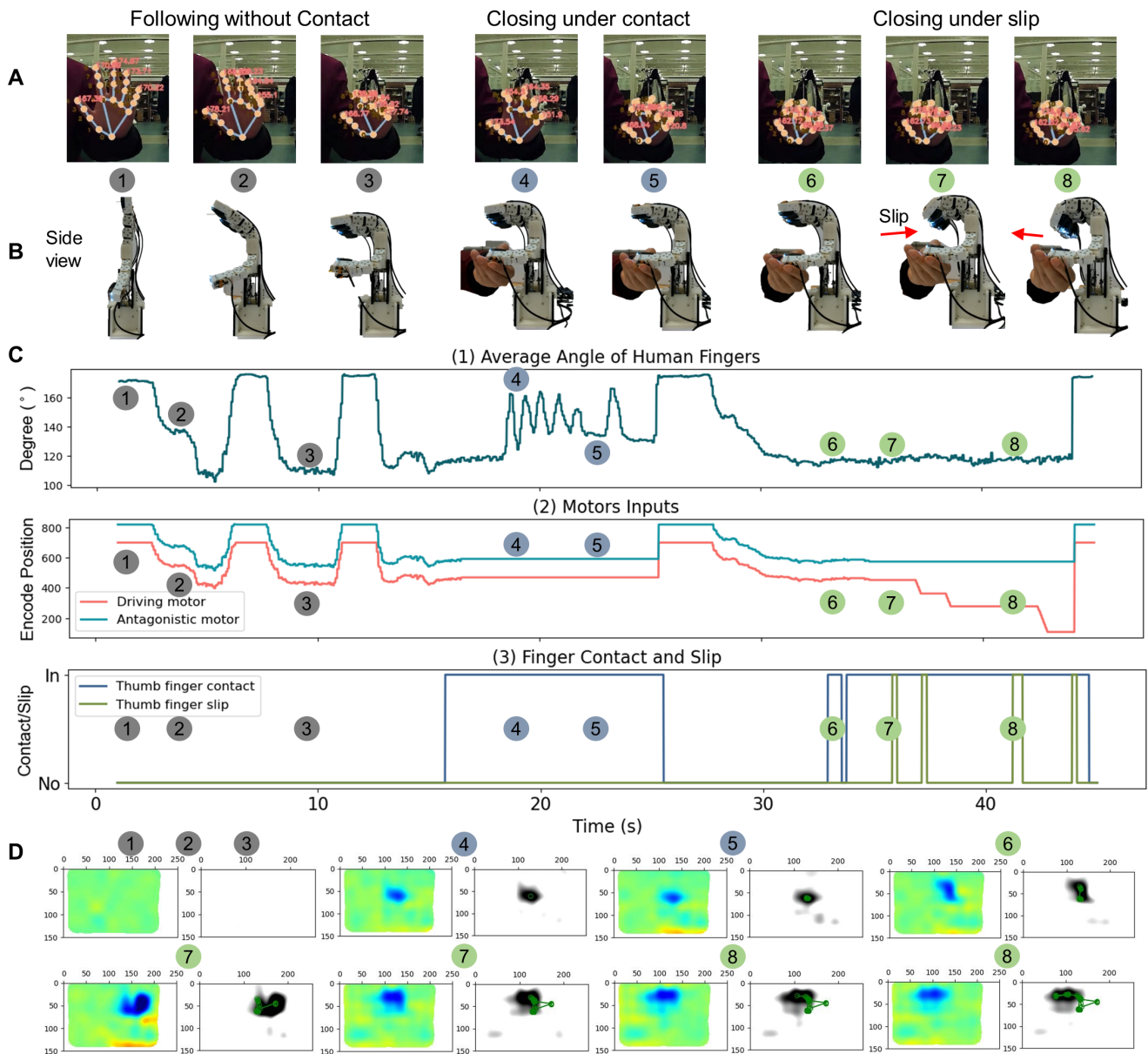


Figure 11. Human gesture and tactile control of the Tactile SoftHand-A. (A) human hand gestures used as inputs to control the hand. (B) side view of Tactile SoftHand-A in response to the gesture control. (C) Average degree of human finger closure (1), corresponding motor inputs to the hand (2) and change of finger contact and slip (3). (D) Tactile contact map at various stages throughout the motion as the hand contacts and object. The results in this figure relate to Experiment D.

gestures. Notably, the delay between these curves is less than one second, attributable to the anti-tendon mechanism in Tactile SoftHand-A, which facilitates rapid response.

From approximately 16 to 26 seconds, the contact stage occurs, during which the thumb's tactile fingertip of Tactile SoftHand-A makes contact with the human hand. Concurrently, contact detection is indicated in Figure 13(C)(3), where the blue curve representing the thumb slip/contact state remains in contact throughout this stage. Additionally, Figure 13(D), images 4-5, depict the contact area and the location of its center point (green circle marker). Furthermore, during this stage, the angle of the human hand's fingers (shown in Figure 13(C)(1)) is deliberately altered to introduce interference, yet the inputs to the two motors are kept constant to preserve the current grasp of Tactile SoftHand-A. This indicates that the control system has engaged in closed-loop tactile feedback control,

unaffected by changes in the human hand's finger angles, thereby enhancing grip stability. The constant gestures of Tactile SoftHand-A are shown in Figure 13(A)(4-5).

From approximately 26 to 33 seconds, the gesture synchronization phase occurs, during which Tactile SoftHand-A is controlled by the human hand to re-establish contact. From 33 to 43 seconds, the slip phase takes place. During this phase, Figure 13(D)(7-8) illustrate the changes in the contact area and the slip of its center point, clearly showing the contact point moving first to the right and then slipping to the left. The green curve in Figure 13(C)(3), which represents slip detection, also remains in the slip state during this period, indicating that slippage has occurred. At same time, the contact is also indicated (blue curve). Following the onset of slippage, the motor inputs change as shown in moments 7 and 8 of Figure 13(C)(2), adjusting the grip gesture of Tactile SoftHand-A by increasing the input differential between the

driving motor and the antagonistic motor. As demonstrated in Figure 13(B)(7-8), the DIP joints of Tactile SoftHand-A's fingers actively rotate inward, adjusting their grip to enhance the gripping force and prevent the object from slipping.

Discussion

The experimental results presented highlight the intricate and precise control mechanisms implemented in the Tactile SoftHand-A, in particular with the D-type finger permitting control of the distal interparietal joint. The key findings from these results are discussed below.

The D-type finger experiments illustrate the effectiveness of coordinated control between the driving and antagonistic motors. By managing the position and tension of the tendons, suitable forces are generated at the PIP and MCP joints that in turn allow for precise control of the DIP joint. This level of control is crucial for tasks requiring fine motor skills, such as changing the hand gesture to prevent slippage while not appreciably increasing the grasping force. The experimental data, depicted in Figure 8D1(a-b), D2(a-b) and D3(a-b), demonstrate the ability of the D-type finger to maintain various degrees of flexion, showing both semi-flexion and full flexion states. The results confirm that the coordinated tendon mechanism effectively controls the finger joints, enhancing the overall dexterity and functionality of the tendon-driven fingers.

The results for the Tactile SoftHand-A in Figure 9 underscore the significance of coordinated motor control in achieving complex hand gestures. By adjusting the encoder values of the driving and antagonistic motors, the DIP joints of all fingers can be controlled, as shown in Figure 9. This method prevents the PIP and MCP joints from active bending, allowing for isolated control of the DIP joints, which is essential for tasks requiring a stable grip while maintaining finger dexterity. The transition from an open hand to a semi-closed and then fully closed hand demonstrates the adaptability of the control system in managing different phases of hand movement.

The adaptability of the Tactile SoftHand-A is further evidenced in grasping experiments with various objects (Figure 10). The thumb's positioning opposite the other fingers allows for effective encircling and stabilization of objects, enhancing the grip's support. The differential mechanism enables each finger to adjust its flexion based on the object's shape, demonstrating a high level of adaptability. This characteristic is particularly important for robot hands that must interact with a variety of objects in daily life. The ability of the fingers to retract and bend independently ensures that the hand can conform to different geometries, improving the practicality and usability of the robot hand.

The tactile feedback mechanism in the Tactile SoftHand-A (Figure 7) highlights the system's ability to synchronize gestures with a human hand and respond to external stimuli. The synchronization phase demonstrates effective mirroring of human hand movements, with a minimal delay attributed to the antagonistic tendon mechanism. The contact and slip detection phases evidence the hand's ability to maintain a stable grasp and adjust to prevent slippage. This closed-loop tactile feedback control is crucial for tasks that require a secure grip, such as holding delicate objects or performing

precision tasks. The ability to detect and respond to slippage ensures that the robot hand can adapt to dynamic conditions, enhancing its functionality and reliability.

Conclusion

The experimental results provide evidence of the advanced control mechanisms and adaptability of the Tactile SoftHand-A. The coordinated control of driving and antagonistic motors allows for precise manipulation of finger joints, while the differential mechanism enhances grasping adaptability. The tactile feedback system further improves the hand's responsiveness and stability in real-world scenarios. These findings contribute to the development of more dexterous and functional minimally-actuated tendon-driven robot hands, capable of performing a wide range of tasks with precision and reliability. Future work could focus on refining these control mechanisms and exploring their applications in dexterous manipulation tasks. Further, because the hand is 3D-printed, different combinations of driving and antagonistic mechanisms coupled with the degree of actuation can be explored. This opens up a rich research area of adding greater dexterity to minimally-actuated anthropomorphic robot hands, so that it becomes possible to investigate systematically how to develop low-cost, minimally actuated hands with evermore human-like dexterity. To this end, we openly release all designs and fabrication instructions for creating the Tactile SoftHand-A as an enabler for others to build upon this work.

Funding

HL, CL and YL were supported by China Scholarship Council (CSC) and Bristol joint scholarship. NFL was supported by a research leadership award from the Leverhulme Trust: 'A Biomimetic Forebrain for Robot Touch' (RL-2016-039). CJF, EP and NFL were supported by the European Union's Horizon Europe program under Grant Agreement No 101120823 ('MANiBOT: Advancing the physical intelligence and performance of roBOTs towards human-like bi-manual objects MANipulation').

References

- Bicchi A, Gabbicini M and Santello M (2011) Modelling natural and artificial hands with synergies. *Philosophical Transactions of the Royal Society B: Biological Sciences* 366(1581): 3153–3161.
- Butterfaß J, Grebenstein M, Liu H and Hirzinger G (2001) Dlr-hand ii: Next generation of a dextrous robot hand. In: *Proceedings 2001 ICRA. IEEE International Conference on Robotics and Automation (Cat. No. 01CH37164)*, volume 1. IEEE, pp. 109–114.
- Catalano MG, Grioli G, Farnioli E, Serio A, Piazza C and Bicchi A (2014) Adaptive synergies for the design and control of the pisa/iit soft-hand. *The International Journal of Robotics Research* 33(5): 768–782.
- Chen F, Xu W, Zhang H, Wang Y, Cao J, Wang MY, Ren H, Zhu J and Zhang Y (2018) Topology optimized design, fabrication, and characterization of a soft cable-driven gripper. *IEEE Robotics and Automation Letters* 3(3): 2463–2470.

- Chen W, Xiong C and Yue S (2014) Mechanical implementation of kinematic synergy for continual grasping generation of anthropomorphic hand. *IEEE/ASME Transactions on mechatronics* 20(3): 1249–1263.
- Crisman J, Kanojia C and Zeid I (1996) Grasp: a flexible, easily controllable robotic hand. *IEEE Robotics Automation Magazine* 3(2): 32–38. DOI:10.1109/100.511778.
- Fan S, Gu H, Zhang Y, Jin M and Liu H (2018) Research on adaptive grasping with object pose uncertainty by multi-fingered robot hand. *International Journal of Advanced Robotic Systems* 15(2): 1729881418766783.
- Gao G, Dwivedi A and Liarokapis M (2021) An anthropomorphic prosthetic hand with an active, selectively lockable differential mechanism: Towards affordable dexterity. In: *2021 IEEE/RSJ International Conference on Intelligent Robots and Systems (IROS)*. IEEE, pp. 6147–6152.
- Gioioso G, Salviati G, Malvezzi M and Prattichizzo D (2013) Mapping synergies from human to robotic hands with dissimilar kinematics: an approach in the object domain. *IEEE Transactions on Robotics* 29(4): 825–837.
- Gosselin C, Pelletier F and Laliberte T (2008) An anthropomorphic underactuated robotic hand with 15 dofs and a single actuator. In: *2008 IEEE International Conference on Robotics and Automation*. pp. 749–754. DOI:10.1109/ROBOT.2008.4543295.
- Jacobsen S, Iversen E, Knutti D, Johnson R and Biggers K (1986) Design of the utah/mit dextrous hand. In: *Proceedings. 1986 IEEE International Conference on Robotics and Automation*, volume 3. IEEE, pp. 1520–1532.
- Jiang L, Zeng B, Fan S, Sun K, Zhang T and Liu H (2014) A modular multisensory prosthetic hand. In: *2014 IEEE International Conference on Information and Automation (ICIA)*. IEEE, pp. 648–653.
- Kappasov Z, Corrales JA and Perdereau V (2015) Tactile sensing in dexterous robot hands. *Robotics and Autonomous Systems* 74: 195–220.
- Kim YJ, Song H and Maeng CY (2020) Blt gripper: An adaptive gripper with active transition capability between precise pinch and compliant grasp. *IEEE Robotics and Automation Letters* 5(4): 5518–5525. DOI:10.1109/LRA.2020.3008137.
- Lambeta M, Chou PW, Tian S, Yang B, Maloon B, Most VR, Stroud D, Santos R, Byagowi A, Kammerer G et al. (2020) Digit: A novel design for a low-cost compact high-resolution tactile sensor with application to in-hand manipulation. *IEEE Robotics and Automation Letters* 5(3): 3838–3845.
- Lee YT, Choi HR, Chung WK and Youm Y (1994) Stiffness control of a coupled tendon-driven robot hand. *IEEE Control Systems Magazine* 14(5): 10–19. DOI:10.1109/37.320882.
- Lepora NF (2021) Soft biomimetic optical tactile sensing with the tactip: A review. *IEEE Sensors Journal* 21(19): 21131–21143.
- Li C, Gu X and Ren H (2017) A cable-driven flexible robotic grasper with lego-like modular and reconfigurable joints. *IEEE/ASME Transactions on Mechatronics* 22(6): 2757–2767. DOI:10.1109/TMECH.2017.2765081.
- Li H, Ford CJ, Bianchi M, Catalano MG, Psomopoulou E and Lepora NF (2022) Brl/pisa/iit soffhand: A low-cost, 3d-printed, underactuated, tendon-driven hand with soft and adaptive synergies. *IEEE Robotics and Automation Letters* 7(4): 8745–8751. DOI:10.1109/LRA.2022.3187876.
- Li H, Nam S, Lu Z, Yang C, Psomopoulou E and Lepora NF (2024) Biotactip: A soft biomimetic optical tactile sensor for efficient 3d contact localization and 3d force estimation. *IEEE Robotics and Automation Letters* .
- Lin C, Zhang H, Xu J, Wu L and Xu H (2023) 9dtact: A compact vision-based tactile sensor for accurate 3d shape reconstruction and generalizable 6d force estimation. *IEEE Robotics and Automation Letters* .
- Liow L, Clark AB and Rojas N (2019) Olympic: A modular, tendon-driven prosthetic hand with novel finger and wrist coupling mechanisms. *IEEE Robotics and Automation Letters* 5(2): 299–306.
- Lu C, Tang K, Yang M, Yue T, Li H and Lepora NF (2024) Dexitac: Soft dexterous tactile gripping. *IEEE/ASME Transactions on Mechatronics* .
- Ma R and Dollar A (2017) Yale openhand project: Optimizing open-source hand designs for ease of fabrication and adoption. *IEEE Robotics Automation Magazine* 24(1): 32–40.
- Makino S, Kawaharazuka K, Kawamura M, Asano Y, Okada K and Inaba M (2017) High-power, flexible, robust hand: Development of musculoskeletal hand using machined springs and realization of self-weight supporting motion with humanoid. In: *2017 IEEE/RSJ International Conference on Intelligent Robots and Systems (IROS)*. IEEE, pp. 1187–1192.
- Martin J and Grossard M (2014) Design of a fully modular and backdrivable dexterous hand. *The International Journal of Robotics Research* 33(5): 783–798.
- Mizushima K, Oku T, Suzuki Y, Tsuji T and Watanabe T (2018) Multi-fingered robotic hand based on hybrid mechanism of tendon-driven and jamming transition. In: *2018 IEEE International Conference on Soft Robotics (RoboSoft)*. IEEE, pp. 376–381.
- Mnyusiwalla H, Vulliez P, Gazeau JP and Zeghloul S (2016) A new dexterous hand based on bio-inspired finger design for inside-hand manipulation. *IEEE Transactions on Systems, Man, and Cybernetics: Systems* 46(6): 809–817. DOI:10.1109/TSMC.2015.2468678.
- Mohd Faudzi AA, Ooga J, Goto T, Takeichi M and Suzumori K (2018) Index finger of a human-like robotic hand using thin soft muscles. *IEEE Robotics and Automation Letters* 3(1): 92–99. DOI:10.1109/LRA.2017.2732059.
- Nurpeissova A, Tursynbekov T and Shintemirov A (2021) An open-source mechanical design of alaris hand: A 6-dof anthropomorphic robotic hand. In: *2021 IEEE International Conference on Robotics and Automation (ICRA)*. IEEE, pp. 1177–1183.
- Ozawa R, Kobayashi H and Hashirii K (2014) Analysis, classification, and design of tendon-driven mechanisms. *IEEE Transactions on Robotics* 30(2): 396–410. DOI:10.1109/TRO.2013.2287976.
- Piazza C, Grioli G, Catalano M and Bicchi A (2019) A century of robotic hands. *Annual Review of Control, Robotics, and Autonomous Systems* 2: 1–32.
- Santello M, Bianchi M, Gabiccini M, Ricciardi E, Salviati G, Prattichizzo D, Ernst M, Moscatelli A, Jörntell H, Kappers AM et al. (2016) Hand synergies: integration of robotics and neuroscience for understanding the control of biological and artificial hands. *Physics of life reviews* 17: 1–23.
- Shirafuji S, Ikemoto S and Hosoda K (2014) Development of a tendon-driven robotic finger for an anthropomorphic robotic

- hand. *The International Journal of Robotics Research* 33(5): 677–693.
- Stuart H, Wang S, Khatib O and Cutkosky MR (2017) The ocean one hands: An adaptive design for robust marine manipulation. *The International Journal of Robotics Research* 36(2): 150–166.
- Sun BY, Gong X, Liang J, Chen WB, Xie ZL, Liu C and Xiong CH (2021) Design principle of a dual-actuated robotic hand with anthropomorphic self-adaptive grasping and dexterous manipulation abilities. *IEEE Transactions on Robotics* : 1–19 DOI:10.1109/TRO.2021.3132532.
- Wang T, Geng Z, Kang B and Luo X (2019) Eagle shoal: A new designed modular tactile sensing dexterous hand for domestic service robots. In: *2019 International Conference on Robotics and Automation (ICRA)*. IEEE, pp. 9087–9093.
- Ward-Cherrier B, Pestell N, Cramphorn L, Winstone B, Giannaccini ME, Rossiter J and Lepora NF (2018) The tactip family: Soft optical tactile sensors with 3d-printed biomimetic morphologies. *Soft robotics* 5(2): 216–227.
- Xiong CH, Chen WR, Sun BY, Liu MJ, Yue SG and Chen WB (2016) Design and implementation of an anthropomorphic hand for replicating human grasping functions. *IEEE Transactions on Robotics* 32(3): 652–671.
- Yuan W, Dong S and Adelson EH (2017) Gelsight: High-resolution robot tactile sensors for estimating geometry and force. *Sensors* 17(12): 2762.
- Zhu W, Lu C, Zheng Q, Fang Z, Che H, Tang K, Zhu M, Liu S and Wang Z (2023) A soft-rigid hybrid gripper with lateral compliance and dexterous in-hand manipulation. *IEEE/ASME Transactions on Mechatronics* 28(1): 104–115. DOI:10.1109/TMECH.2022.3195985.

Appendix

Details of Tactile SoftHand-A

Tactile SoftHand-A is powered by two HIWONDER HX-35H motors, which drive the driving tendon and antagonistic tendon, respectively. At 11.1 volts, these motors provide a torque of 25 kg per cm. The entire hand is manufactured using a multi-material 3D printer, the Stratasys J826. The hand's skeleton and most of the opaque solid parts are made from Verowhite material, while the parts resembling acrylic plates are made from Veroclear. Transparent soft tissues and the black tactile epidermis are respectively crafted from Agilus clear and Agilus black.

Details of fully 3D-printed TacTip tactile fingertip

As previously mentioned, the entire tactile fingertip is produced in a single print by a multi-material printer, incorporating white hard phalanges, black soft tactile skin, transparent white filler, white markers, and a transparent hard window. We will release a fabricating instruction that introduces all necessary steps in our website after this work is published.

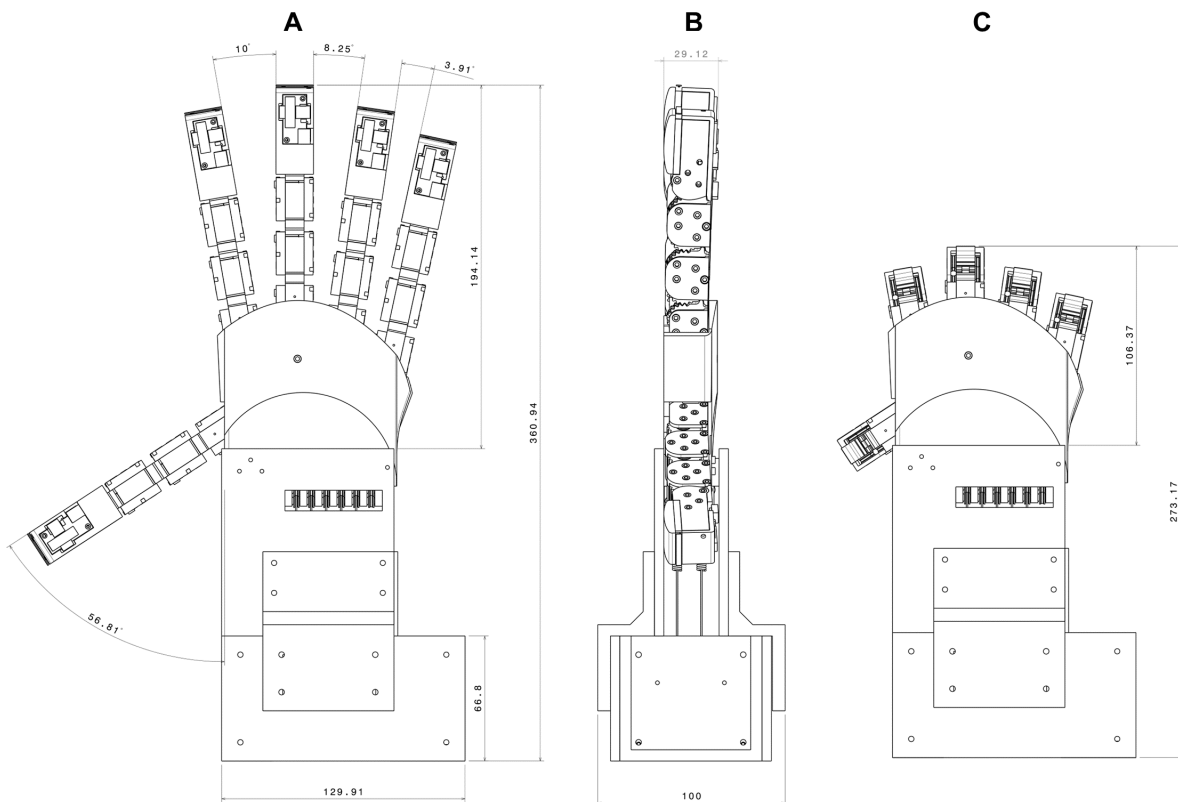


Figure 12. Technical drawing of the Tactile SoftHand-A showing the components and their dimensions. (A) Back view. (B) Left view. (C) Back view of the closed hand.

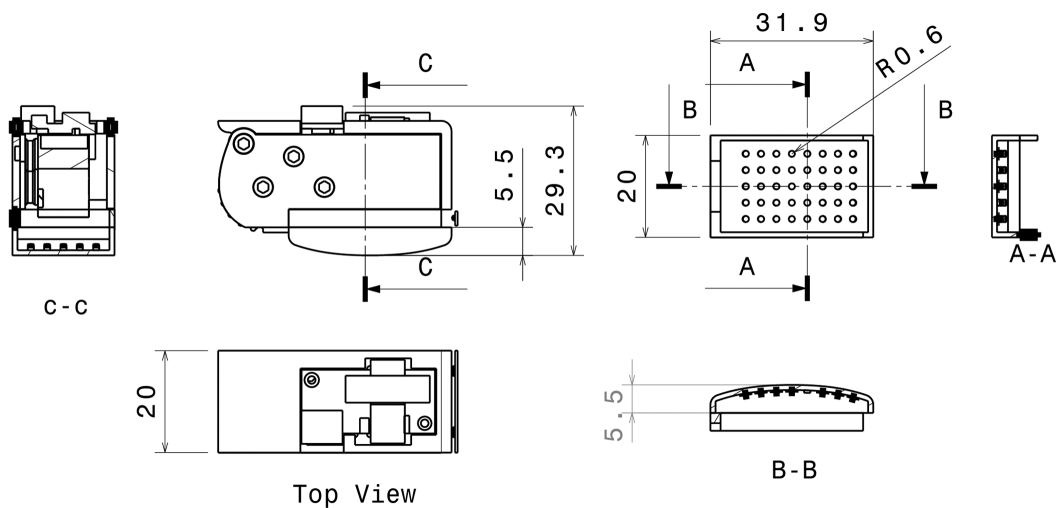


Figure 13. Technical drawing of the tactile fingertip showing all components and their dimensions